ELSEVIER

Applied Surface Science 195 (2002) 146–154

applied surface science

www.elsevier.com/locate/apsusc

Scanning electric field sensing for semiconductor dopant profiling

M.S. Crosser[a,b], S.H. Tessmer[a,b], Ruby N. Ghosh[b,*]

[a]*Department of Physics and Astronomy, Michigan State University, East Lansing, MI 48824-2320, USA*
[b]*Center for Sensor Materials, Michigan State University, East Lansing, MI 48824-2320, USA*

Received 19 October 2001; received in revised form 9 May 2002; accepted 9 May 2002

Abstract

Electric field sensitive scanning probe microscopes (SPMs) can image the electronic properties of a semiconductor through an insulating layer—making the techniques well suited to extract underlying substrate dopant densities. A standard atomic force microscope (AFM) can be used to sense electric field by measuring the electrostatic response of a vibrating cantilever. We have constructed an inexpensive accessory to a commercial AFM to simultaneously acquire images of the spatial variations in substrate doping along with accurate topographic images. Our electric field images have a spatial resolution of 1 μm. In addition, we show explicitly how a simple parallel plate model can be used to extract the magnitude of lateral changes in dopant density from the electric field images. For a substrate doping density of 1×10^{16} cm^{-3} we can discern resistivity changes of ∼1 Ω cm.

PACS: 61.16.Ch; 72.80.Cw; 73.40.Qv

Keywords: Scanning probe microscopy; Electric field imaging; Semiconductor dopant density

1. Introduction

Capacitance measurements of gated semiconductor devices represent a well-established technique to extract dopant densities. As silicon devices become smaller, however, the need for non-destructive profiling methods over microscopic areas becomes increasingly important. There is a need to determine changes in substrate dopant density below an oxide overlayer for quality control of metal-oxide-semiconductor (MOS) field-effect transistors (FETs) [1], especially as channel lengths decrease in state of the art devices. Scanning probe microscopes (SPMs), which can image the electronic properties of a semiconductor surface through an insulating layer [2] are well suited to this task.

Although scanning capacitance microscopes (SCMs) [3–7] are available commercially as individual units or attachments to larger SPM systems, the cost of such systems can be prohibitive. In this paper, we present a comprehensive method to acquire high-quality electric field images using a commercial microscope [8] in conjunction with a home-built accessory. Images of samples with spatially varying dopant density, but no topographical contrast were obtained. These images reveal how the derivative of capacitance with respect to tip/sample separation, dC/dz, varies with the underlying changes in dopant densities. We explicitly show how a parallel plate capacitor model (Fig. 1) can be used to extract to

* Corresponding author. Tel.: +1-517-432-5547; fax: +1-517-432-5501.
E-mail address: ghosh@pa.msu.edu (R.N. Ghosh).

0169-4332/02/$ – see front matter
PII: S0169-4332(02)00538-X

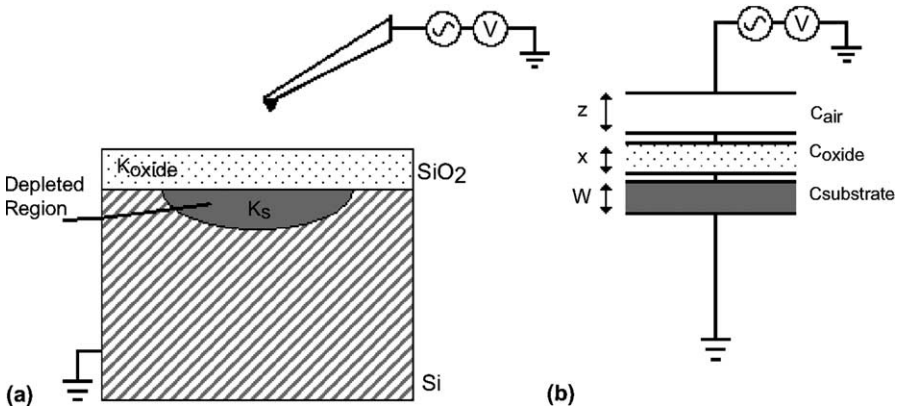

Fig. 1. (a) Schematic of tip to sample geometry; (b) parallel plate capacitors in series to model the electrostatic interactions.

first order changes in dopant density from the measured signal.

A standard function of commercial atomic force microscopes (AFMs) is the Kelvin probe measurement [9]. This technique is able to detect dC/dz, which is a function of the electric field, by measuring the electrostatic force on the tip. Using this basic approach, we have developed a technique to independently vary the dc sample potential to extract the semiconductor properties from the dC/dz images. For both Kelvin probe and electric field imaging, one applies an ac potential with amplitude V_{ac} at a frequency $f = \omega/2\pi$ and a dc offset to the probe $V = V_{dc} + V_{ac}\sin(\omega t)$ (Fig. 1(a)). The force on the probe is derived from finding the gradient of the energy of a capacitor system [10]:

$$F = \frac{1}{2}\frac{dC}{dz}\left(V_{dc}^2 + \frac{1}{2}V_{ac}^2 + 2V_{ac}V_{dc}\sin(\omega t) - \frac{1}{2}V_{ac}^2\cos(2\omega t)\right). \quad (1)$$

These techniques use the topography measured by a tapping atomic force microscope (TAFM) in order to keep a constant distance from the surface. After each line in tapping mode, a second line is scanned in "lift" mode following the topography but raised an additional height specified by the user. Note that V_{dc} includes both the user applied potential and a component due to the contact potential.

The probe is attached to a cantilever that responds most to the oscillating force if the ac excitation frequency matches its resonant frequency. By operating the ac excitation at the resonant frequency of the tip, the oscillating amplitude will be dominated by the force of the one-omega term, the middle term with both ac and dc potentials in Eq. (1). The response due to the last term, the two-omega term, will be much less than the one-omega excitation and may be ignored. The first two terms account for a dc attraction to the surface, which will bend the tip closer to the surface for large potentials, but will not add any oscillatory response.

In typical Kelvin probe operation, the user controls an ac input but has no control over the dc potential, which is set by a feedback loop to keep the amplitude of the cantilever zero. However, in order to image the electronic properties of the semiconductor surface, one must be able to independently apply a dc potential to deplete the semiconductor without distorting AFM topographical data—necessary to maintain a constant tip to sample separation. We have therefore designed an external power source to apply a dc potential to the sample and to disable the feedback loop. By controlling the ac component through the standard control electronics and the dc through the external source, one can measure the amplitude of the probe oscillation to obtain dC/dz images.

The semiconductor carrier concentration can be determined from the dC/dz images under the appropriate bias conditions. Using a metal-coated probe tip in lift mode the probe/sample system can be regarded as a MOS capacitor with an additional series capacitance due to the tip/sample air gap (Fig. 1). Consider

the case where the sample is biased in inversion and the ac modulation frequency is faster than the minority carrier generation–recombination rate. The sample capacitance is then the series combination of the oxide plus semiconductor capacitance, which is in turn a function of the substrate doping density.

2. External voltage module

Our first generation of the external potential source involved a simple voltage source with variable resistors to control the dc offset. This dc was then fed back into the microscope and to the probe. Unfortunately, this design affected the tapping mode of the microscope for dc potentials larger than about 1 V. Apparently, changes in electrostatic forces between the charged probe and underlying layers contributed significantly to the measured topography. For example, topographical steps could be created on flat surfaces when large dc biases were applied. These false steps then distorted subsequent dC/dz images. Using a triggered voltage source solved this problem. The final design (Fig. 2) uses the input of the tapping signal to toggle the dc potential.

The triggered voltage source works as follows. The tapping signal (labeled Ana_1) is first rectified then amplified and sent through a Schmitt Trigger, which interprets the signal as a digital input. The Schmitt Trigger then inverts the logical signal and outputs either 0.005 V when the microscope runs in tapping mode, or 2.3 V when the microscope is in lift mode. Therefore, the analog signal from the microscope is transformed into a stable digital dc signal. This dc signal is then amplified to the range 0.02–9 V. It is then adjusted by a potentiometer connected to ground and sent through two inverting buffers before being sent to the output. A switch at the output of each buffer enables the user to choose either a positive or negative bias, allowing a full range of -9 to $+9$ V. This dc potential is added to Ana_2, the ac signal from the microscope, and sent to the probe through an RC filter. Although the 'low' output still applies a small potential to the tip, no effect is evident in the tapping mode of the microscope.

3. Sample preparation/procedure

The imaging capabilities of the system were studied using Si samples patterned with alternating stripes of p-type dopant. The initial Si wafer was doped with 1×10^{16} cm^{-3} of boron. Stripes of higher boron doping density were implanted through a mask consisting of 5 μm wide parallel slits, followed by an implantation anneal at 900 °C for 10 min [11]. An ∼20 nm thick thermal oxide was then grown to gate the semiconductor carrier concentration. The oxide thickness was determined using spectroscopic ellipsometry.

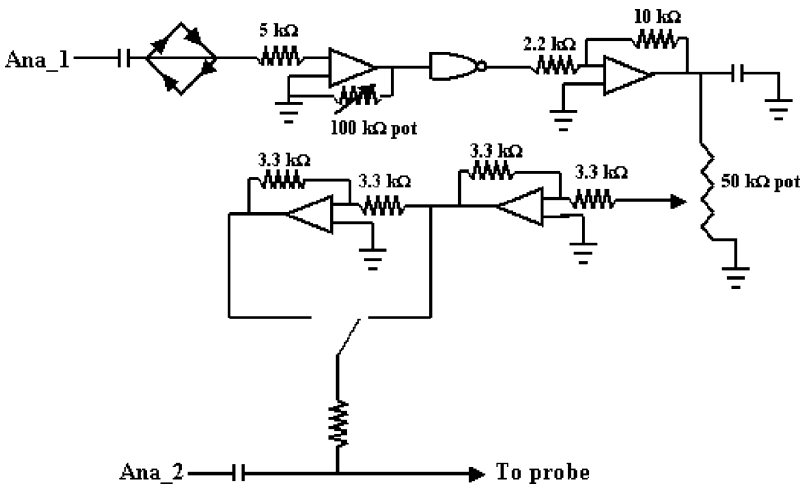

Fig. 2. Circuit diagram of the triggered external power supply with inputs of Ana_1 (tapping amplitude) and Ana_2 (ac excitation) and an output sent to probe.

Table 1
Summary of the electrical properties of the three test samples

Sample	Implant density (cm^{-3})	Resistivity (Ω cm)	Oxide thickness (nm)
P1	6×10^{17}	0.07	21.8
P2	6×10^{18}	0.02	21.7
P3	6×10^{19}	0.002	20.7
Substrate	1×10^{16}	1.3	–

Finally, a layer of gold was deposited on the reverse side to provide a back contact. Table 1 summarizes the details of the resultant three samples. Microscopy of the samples was performed in a clean room environment, where the humidity was controlled and the ambient room temperature was held constant to within 1 °C. Prior to imaging, the samples were regularly immersed in a solvent bath to ensure clean surfaces; nevertheless, some contaminants were still evident due to handling.

For the simultaneously obtained topographical and electric field images, commercially purchased metal-coated tips [8], with resonant frequencies near 65 kHz, were used. The integral and proportional gains were chosen to produce the cleanest TAFM image prior to starting the lift mode. As expected, the signal amplitude varied linearly with the ac potential. Therefore, V_{ac} was chosen to produce a large signal while being sufficiently small compared to V_{dc}, so as to not significantly alter the dc sample potential. The lift height was optimized for each sample and ranged from 50 to 100 nm. Note the lift height will be the upper bound on the tip to sample separation used in the model below, since electrostatic forces will tend to attract the probe closer to the surface.

4. Measurements

In Fig. 3, we show a topographical image of P1 and dC/dz images of each test sample. The dC/dz images were obtained using $V_{ac} = 0.5$ V, a scan rate of 0.751 Hz per line, and sample specific values for both V_{dc} and lift height. We focus first on the simultaneously obtained dC/dz and topographic images of sample P1, Fig. 3(a) and (b), respectively. As expected, the surface of the oxide is flat, showing no variations in oxide thickness due to the underlying changes in substrate doping level. The rms roughness is 0.43 nm, with a few isolated features that are less than 5 nm tall. Notice that sharp spikes in the topography are displayed in the lift mode as decreased signal. As shown in Fig. 3(b), we can clearly image changes in doping density between 1×10^{16} and 6×10^{17} cm^{-3}, which corresponds to a change in resistivity of 1.2 Ω cm.

These images demonstrate that the technique is well suited for measuring the electronic properties of buried semiconductor surfaces beneath an insulating layer with no other topographical evidence. The dC/dz image in Fig. 3(b) had been plane subtracted and had line-by-line correction (flattened) to compensate for drift effects. The image was then inverted, since the original signal was subtracted from a reference point. No other processing was required for these images, in contrast to typical TAFM images.

Fig. 3(c) and (d) shows the dC/dz images of two samples with higher implanted doping densities of 6×10^{18} and 6×10^{19} cm^{-3}. The alternating p/p+ stripes are well resolved. These two samples had more surface roughness than P1, as the black spots are more prevalent in these images compared to the image of P1. Identical image processing was used to display these images as that for Fig. 3(b). All three images are plotted on the same scale, but the amplitudes of the signals are not directly comparable, since each image was made under slightly different conditions. The inferior image quality is due primarily to the rough topography of the oxide overlayer; indeed, we find clean, flat surfaces work best for this technique.

The signal to noise ratio for samples P1 and P2 is about 6:1. Since data is acquired every 2–3 ms, this corresponds to a noise level equal to 0.0003 pF/$(m\sqrt{Hz})$.

The SNR for sample P3, which yielded a much smaller signal than the other two samples, is only about 2:1. To quantify the capabilities of our technique, we show in Fig. 4 the minimal resolvable implant dopant density as a function of substrate doping. This figure was generated assuming a SNR of 2 and using the results of the model described in the next section. From our images (see Fig. 3), we extrapolate that dC/dz imaging would be able to resolve changes in doping density from 1×10^{16} to 3×10^{16} cm^{-3}, a change in resistivity of 1 Ω cm. At even lower concentration, for example 1×10^{14} dopants per cm^3, we could

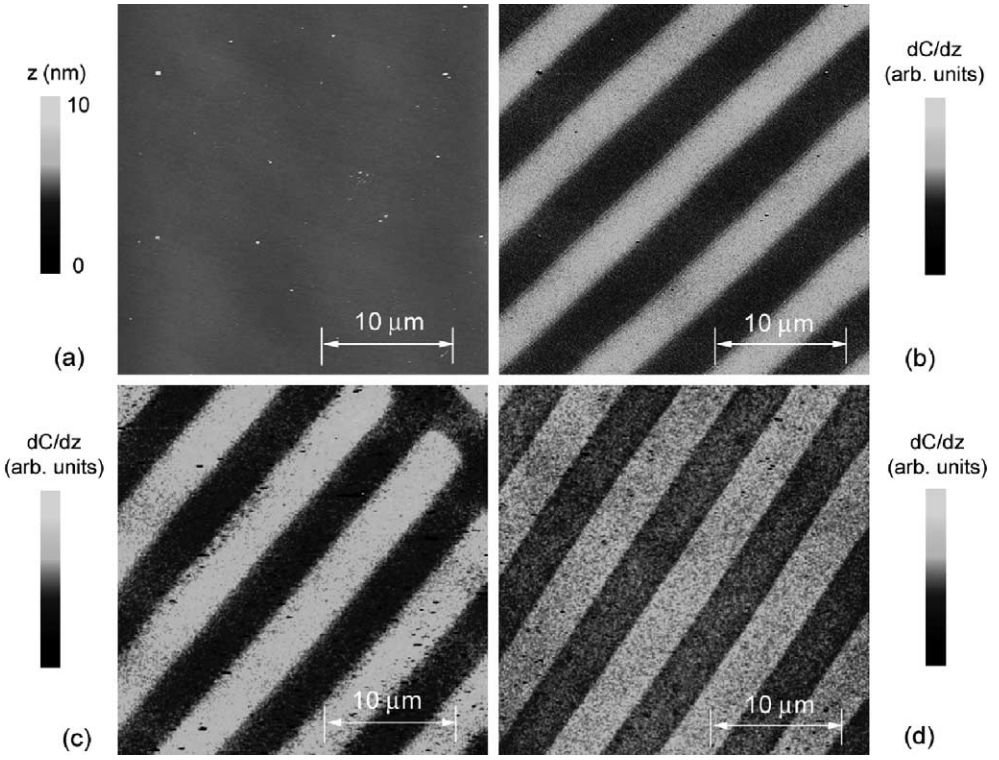

Fig. 3. (a) Topographical image of sample P1; all features are less than 5 nm tall. (b–d) Examples of dC/dz images from samples P1–P3, respectively. For image (b), acquired concurrently with image (a), the lift height was 55 nm with +3 V dc applied to the probe. For images (c and d), the parameters were 70 nm/+3 V and 100 nm/+5 V, respectively.

resolve changes in dopant density between 1×10^{14} and 8×10^{14} cm^{-3}, a change in conductivity of only 10%. Therefore, dC/dz imaging is well suited to characterize samples with low doping densities.

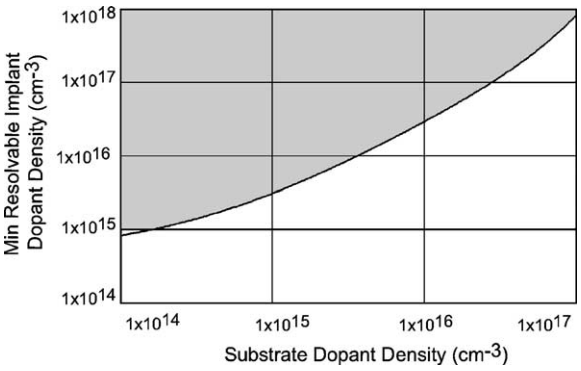

Fig. 4. Extrapolated minimal resolvable implant dopant density, for a SNR of 2. Any implant within the shaded region would be resolvable via dC/dz imaging.

To investigate the reproducibility of the system, measurements were made on the same sample with similar operator defined conditions, but on different days with different tips. Shown in Fig. 5 are two different images of sample P1 along with the corresponding line scans. From the 20–80% level of the signal we see from the line scans that the dC/dz technique can resolve changes in doping density with a 1 μm lateral resolution. This result is comparable to that obtained from SCM images of implanted/furnace annealed Si samples.[1]

The data were acquired with metal-coated tips that were used for less than 20 h before the images were scanned. Older tips tended to behave more unpredictably than newer ones, presumably because worn probes drastically changed the geometry of system. The use of highly doped Si tips was also attempted. The Si tips were less expensive, able to last longer

[1] See Fig. 3 of [3].

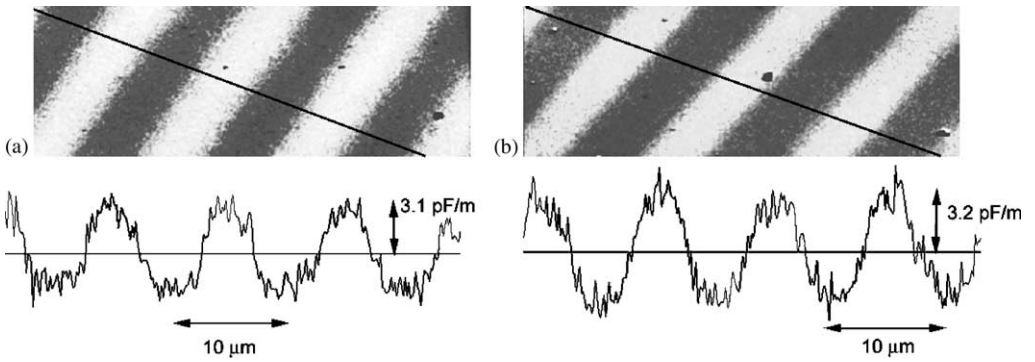

Fig. 5. Demonstration of the reproducibility of dC/dz imaging on sample P1: (a) image and line scan with 3 V ac and a cantilever frequency of 63 kHz; (b) image and line scan with 3 V ac and frequency of 62 kHz, taken 1 month prior to image (b). The line scans correspond to a cross-section of each image along the dashed line.

[12], and capable of producing clearer topographical images. However, the larger radii and better conduction of the metal-coated tips yielded better SNR in the lift mode than the Si tips. The difference in step heights between Fig. 5(a) and (b) is less than 5%. We typically obtain dC/dz images that differ by about 10% from day to day on the same sample. Given the inherent tip-to-tip variation, such differences are expected.

5. Model to extract semiconductor dopant densities

To extract the semiconductor dopant densities from the dC/dz images, we must develop a model of the electrostatic interactions between the tip and the sample. From the model, we can determine the contribution of the semiconductor to the form of dC/dz. Inserting this form of dC/dz into Eq. (1) allows us to calculate the sample contribution to the force in the tip. Lastly, one must determine how the cantilever responds to the force. By assuming the cantilever is a mass-less spring driven by this force we can determine the amplitude of its oscillations, the experimentally measured quantity. Other researchers have made similar models [13].

The actual form for the capacitive interaction of the probe and the sample is quite complex (Fig. 1(a)), since the geometry includes an irregular cone-shaped probe held on a cantilever angled above a flat surface. For the ac interactions, the cone is the most important shape, while the cantilever is most responsible for the dc response. Because of the complicated geometry, let us use a first order approximation to solve the system. By modeling the system as parallel plate capacitors (Fig 1(b)) held by massless springs, this dC/dz signal can be converted into an estimate of the spatial variation in doping density. As shown in Fig. 1(b), the parallel plate analysis creates three regions with distinct capacitances that will affect the dC/dz of the signal. These regions are represented by the probe to sample distance C_{air} (lift height), oxide thickness C_{ox}, and depletion width C_{s} (a function of dopant density and dc potential). Since the probe follows the topography of the sample from tapping AFM mode, the lift height may be considered constant in the dC/dz measurement. Furthermore, the topography changes for our samples were very small (less than 1 nm), so changes in oxide thickness were ignored.

As long as the tip is not raised above ~100 nm, the parallel plate model predicts results very close to more extensive models [14]. Since the ac modulation frequency is > 60 kHz, we assume that we are in the high-frequency limit. Therefore, the sample capacitance is given by the sum of the oxide and semiconductor capacitances when biased in inversion. Using a parallel plate model and the delta depletion approximation [15], we see the total tip to sample capacitance is

$$C = \left(\frac{1}{C_{\text{air}}} + \frac{1}{C_{\text{ox}}} + \frac{1}{C_{\text{s}}}\right)^{-1}, \qquad C_{\text{air}} = \frac{A\varepsilon_0}{z},$$
$$C_{\text{ox}} = \frac{A\kappa_{\text{ox}}\varepsilon_0}{x}, \qquad C_{\text{s}} = \frac{A\kappa_{\text{s}}\varepsilon_0}{W}. \tag{2}$$

Here, A is chosen as the area of a circle with radius equal to the nominal radius for our commercial probe, $\pi(50\,\text{nm})^2$. The permittivity of free space, ε_0, is 8.85×10^{-14} F/cm. The oxide thickness of each sample, x, was measured with a spectroscopic ellipsometer. The tip to surface distance, z, was chosen as the user-defined lift height plus the equilibrium tip to surface separation in tapping mode. Holding all other values constant, we assume the semiconductor is fully depleted below the tip such that the depletion width is given by:

$$W = W_{\max}\left[\frac{4\kappa_s\varepsilon_0 k_B T}{q^2 N_A}\ln\left(\frac{N_A}{n_i}\right)\right]^{1/2}, \tag{3}$$

where q is the electron charge, $\kappa_s = 11.9$ the dielectric constant for silicon, $T = 291$ K (ambient room temperature), the Boltzmann constant, $k_B = 1.38 \times 10^{-23}$ J/K, $n_i = 1 \times 10^{10}$ cm^{-3} is the carrier density of intrinsic silicon, and N_A is the carrier concentration. In this geometry, the derivative of the capacitance is clearly proportional to C^2:

$$F \propto \frac{dC}{dz} = \frac{d}{dz}\left(\frac{1}{C_{air}} + \frac{1}{C_{ox}} + \frac{1}{C_s}\right)^{-1} = \left(\frac{1}{C_{air}} + \frac{1}{C_{ox}} + \frac{1}{C_s}\right)^{-2}\frac{1}{A\varepsilon_0} = \frac{C^2}{A\varepsilon_0}. \tag{4}$$

The probe is attached to a cantilever that responds to the force created by the moving charges. Assuming the cantilever is a massless spring attached to the probe, from elementary physics, one knows

$$\ddot{x} + 4\pi\beta\dot{x} + \omega_0^2 x = \frac{F_0}{m}\cos\omega t,$$

$$\text{where } F_0 = \frac{dC}{dz}V_{dc}V_{ac}. \tag{5}$$

F_0 is the amplitude from Eq. (1), ω_0 the resonant frequency measured by the microscope, the damping coefficient β is extracted from the width of a resonance curve, and $m = k\omega_0^2$ where k is nominal spring stiffness reported by the probe manufacturer. The solution for this equation is $x_p = D\cos(\omega t - \delta)$, where $D/\sqrt{2}$ is the rms amplitude of the oscillations, as recorded by the microscope [16]. The amplitude of displacement caused by the driving force can be solved in terms of the spring's resonant frequency ω_0 as:

$$D = \frac{V_{ac}V_{dc}(dC/dz)}{m\sqrt{4\omega^2\beta^2 + (\omega_0^2 - \omega^2)^2}}. \tag{6a}$$

Both V_{ac} and V_{dc} are values entered by the user. Now, by performing the experiment so that the driving frequency is equal to the resonant frequency, this equation simplifies to

$$D = \frac{V_{ac}V_{dc}}{8\pi^2 M v\beta'}\frac{dC}{dz}. \tag{6b}$$

This solution gives the amplitude of the oscillations in meters. A conversion can be found experimentally which maps this answer to volts, which is the output quantity of the microscope [17].

To test the validity of this model, we compared it to the data from sample P1. While both the dC/dz images of samples P2 and P3 show well-defined contrast due to the variations in dopant level, we find that the approximations made in the model are not appropriate in these cases. The implanted regions in P2 and P3 are degenerately doped. The approximation of the tip as a small parallel plate neglects the capacitance of the macroscopic cantilever (200 μm in length). For a degenerately doped sample, the resulting dc electrostatic force on the cantilever significantly shifts its equilibrium position towards the sample.

6. Discussion

Table 2 lists all of the user-controlled variables used to model sample P1. The model predicts that the

Table 2
Summary of the data used to model the change in the dC/dz signal for sample P1

Variable	Value
Substrate density	1×10^{16} cm^{-3}
Implant density	6×10^{17} cm^{-3}
dc voltage	+3 V
ac voltage	0.5 V
z	55 nm
Resonant frequency	62.1 kHz
Damping coefficient	200 Hz
Spring stiffness	3 N/m
Ambient temperature	291 K
Tip radius	50 nm
Surface area	8×10^{-15} m^2
Oxide thickness	21.8 nm
Amplitude coefficient	0.022 V/nm
Theoretical amplitude	0.43 nm
Experimental amplitude	0.48 ± 0.08 nm

difference in signal amplitude between the substrate and implanted regions is 0.43 nm. Experimentally, we extract 0.48 ± 0.08 nm from the dC/dz images. We found that, whereas the relative change in amplitude is constant, other instabilities and drifts of the microscope were too great to enable extraction of absolute capacitance values, even when the system ran for over 2 h prior to recording data.

Within this model, there are two additional factors one must take care to consider. First, the same dc potential will not reach the sample uniformly as the probe scans across it. Following the parallel plate model, we see that regions doped higher will have a thinner depletion width and therefore smaller impedances than less doped regions. This difference in impedance reduces the potential of the Si/SiO2 interface compared to that for the less doped region. The dc potential of the surface follows the simple relation $V_{\text{surface}}(C_{\text{s}} + C_{\text{above}}) = V_{\text{applied}}$. C_{s}, is the summation of C_{air} and C_{ox} in series. Therefore, since the model assumes the semiconductor is fully depleted, the measured signal should be larger than predicted. Another consideration is the fact that the probe height above the surface is not fixed. Notice in the force equation that the first two terms add a constant attraction of the tip to the sample. For large potentials, this attraction will cause the probe to hit the surface, changing the amplitude of oscillations in the output. Therefore, one must be careful to apply a large enough potential to deplete the sample, but not large enough to cause probe/sample interference. This balance is more difficult to reach for more heavily doped samples; therefore, this technique will work best for samples with lower dopant densities. This effect, in addition to the fact that the amplitude depends linearly on V_{dc}, makes a plot of dC/dz versus V from inversion to depletion difficult. Given that this model is a first order approximation and the limitations discussed above, a 10% agreement between model and experiment is surprising.

As indicated in Eq. (1), it should be possible also to use an ac excitation that is equal to one-half of the resonant frequency of the tip. Doing so will cause the two-omega term to excite the tip, rather than the one-omega term used in the calculations. In the two-omega term, the dc potential does not directly induce an ac component to the force on the probe, making measurements independent of a direct dc signal. Unfortunately, this component of force is inherently a quarter of the signal of the one-omega term. Therefore, large ac amplitudes are required to see a signal. Since larger ac amplitudes tend to ''smear'' the voltage scale of the C–V characteristics of devices, the use of an ac component at one-half the resonant frequency was not feasible in our measurements.

7. Conclusion

In summary, we have presented an inexpensive modification of a commercial AFM that enables simultaneous topographical and electric field imaging. With an applied ac and dc potentials to the probe, we precisely measure the probe oscillation, which is proportional to dC/dz. By modeling the electrostatic interactions between the tip and the sample, the electronic properties of the semiconductor surface are extracted. The spatial resolution of our image is 1 μm. For a substrate doping density of 1×10^{16} cm^{-3} 1 Ω cm; the technique is well suited to characterize samples with low doping density. The images were obtained from oxidized Si samples with no topographical contrast, demonstrating that dC/dz imaging is a fast way to determine dopant densities of buried semiconductor surfaces.

Despite the operating restrictions of this system, if one is able to account for the electrostatic interactions correctly, it is a less costly alternative to purchasing commercial packages. Our accessory costs about US$ 200 while the commercial upgrade costs US$ 30,000. Furthermore, since this system uses a tapping AFM rather than a contact AFM to maintain a constant tip/sample separation, it is a better choice for samples with large features or soft surfaces.

Acknowledgements

The authors would like to acknowledge J.J. Kopanski for providing the Si samples and sustained technical input towards this project. For their interest and advice, our gratitude goes toward D. Reinhard, B. Bi, S. Urazhdin, P. Tobias, C. Moreau, and M. Bruening. This work was supported by the MRSEC program of the National Science Foundation Award No. DMR-9809688. SHT acknowledges support of the Alfred P. Sloan Foundation.

References

[1] S. M. Sze, Physics of Semiconductor Devices, Wiley, New York, 1981.
[2] C.C. Williams, Two-dimensional dopant profiling by scanning capacitance microscopy, Annu. Rev. Mater. Sci. 29 (1999) 471–504.
[3] C.C. Williams, J. Slinkman, W.P. Hough, H.K. Wickramasinghe, Lateral dopant profiling with 200 nm resolution by scanning capacitance microscopy, Appl. Phys. Lett. 55 (16) (1989) 1662–1664.
[4] J.J. Kopanski, J.F. Marchiando, D.W. Berning, R. Alvis, H.E. Smith, Scanning capacitance microscopy measurement of two-dimensional dopant profiles across junctions, J. Vac. Sci. Technol. B 16 (1) (1998) 339–343.
[5] R.N. Kleiman, M.L. O'Malley, F.H. Baumann, J.P. Garno, G.L. Timp, Scanning capacitance microscopy imaging of silicon metal-oxide-semiconductor field effect transistors, J. Vac. Sci. Technol. B 18 (4) (2000) 2034–2038.
[6] H. Edwards, V.A. Ukraintsev, R. San Martin, F.S. Johnson, P. Menz, S. Walsh, S. Ashburn, K.S. Wills, K. Harvey, M.C. Chang, pn-Junction delineation in Si devices using scanning capacitance spectroscopy, J. Appl. Phys. 87 (3) (2000) 1485–1495.
[7] F. Giannazzo, L. Calcagno, V. Raineri, L. Ciampolini, M. Ciappa, E. Napolitani, Quantitative carrier profiling in ion-implanted 6H–SiC, Appl. Phys. Lett. 79 (8) (2001) 1211–1213.
[8] Digital Instruments Dimension 3100 Scanning Probe Microscope, Santa Barbara, CA.
[9] M. Nonnenmacher, M.P. O'Boyle, H.K. Wickramasinghe, Kelvin probe force microscopy, Appl. Phys. Lett. 58 (25) (1991) 2921–2923.
[10] F. Muller, A.-D. Muller, M. Hietschold, S. Kammer, Detecting electrical forces in noncontact atomic force microscopy, Meas. Sci. Technol. 9 (1998) 734–738.
[11] G. Neubauer, A. Erickson, C.C. Williams, J.J. Kopanski, M. Rodgers, D. Adderton, Two-dimensional scanning capacitance microscopy measurements of cross-sectioned very large scale integration test structures, J. Vac. Sci. Techol. B 14 (1) (1996) 426–432.
[12] H.O. Jacobs, H.F. Knapp, A. Stemmer, Practical aspects of Kelvin probe force microscopy, Rev. Sci. Inst. 70 (3) (1999) 1756–1760.
[13] M. Yves, D.W. Abraham, H.K. Wickramshinghe, High-resolution capacitance measurement and potentiometry by force microscopy, Appl. Phys. Lett. 52 (3) (1988) 1103–1105.
[14] S. Belaidi, P. Girard, G. Leveque, Electrostatic forces acting on the tip in atomic force microscopy: modelization and comparison with analytic expressions, J. Appl. Phys. 81 (3) (1997) 1023–1030.
[15] R.F. Pierret, Field Effect Devices, Vol. IV, Addison-Wesley, Reading, MA, 1990.
[16] G.F. Simmons, Differential Equations with Applications and Historical Notes, McGraw-Hill, New York, 1991, pp. 111–112.
[17] Nanotips, Editorial, Nanovations 6 (2000) 1.